Biochimica et Biophysica Acta 1807 (2011) 95–107

Contents lists available at ScienceDirect

Biochimica et Biophysica Acta

journal homepage: www.elsevier.com/locate/bbabio

Experimental evidence that the membrane-spanning helix of PufX adopts a bent conformation that facilitates dimerisation of the *Rhodobacter sphaeroides* RC–LH1 complex through N-terminal interactions

Emma C. Ratcliffe [a], Richard B. Tunnicliffe [a], Irene W. Ng [a], Peter G. Adams [a], Pu Qian [a], Katherine Holden-Dye [b], Michael R. Jones [b], Michael P. Williamson [a], C. Neil Hunter [a,*]

[a] Department of Molecular Biology and Biotechnology, University of Sheffield, Sheffield S10 2TN, UK
[b] Department of Biochemistry, School of Medical Sciences, University of Bristol, University Walk, Bristol, BS8 1TD, UK

ARTICLE INFO

Article history:
Received 12 July 2010
Received in revised form 27 September 2010
Accepted 4 October 2010
Available online 16 October 2010

Keywords:
Bacterial photosynthesis
PufX, light harvesting
Reaction center
Membrane protein
Photosynthetic membrane

ABSTRACT

The PufX polypeptide is an integral component of some photosynthetic bacterial reaction center-light harvesting 1 (RC–LH1) core complexes. Many aspects of the structure of PufX are unresolved, including the conformation of its long membrane-spanning helix and whether C-terminal processing occurs. In the present report, NMR data recorded on the *Rhodobacter sphaeroides* PufX in a detergent micelle confirmed previous conclusions derived from equivalent data obtained in organic solvent, that the α-helix of PufX adopts a bent conformation that would allow the entire helix to reside in the membrane interior or at its surface. In support of this, it was found through the use of site-directed mutagenesis that increasing the size of a conserved glycine on the inside of the bend in the helix was not tolerated. Possible consequences of this bent helical structure were explored using a series of N-terminal deletions. The N-terminal sequence ADKTIFNDHLN on the cytoplasmic face of the membrane was found to be critical for the formation of dimers of the RC–LH1 complex. It was further shown that the C-terminus of PufX is processed at an early stage in the development of the photosynthetic membrane. A model in which two bent PufX polypeptides stabilise a dimeric RC–LH1 complex is presented, and it is proposed that the N-terminus of PufX from one half of the dimer engages in electrostatic interactions with charged residues on the cytoplasmic surface of the LH1α and β polypeptides on the other half of the dimer.

1. Introduction

The PufX polypeptide is an integral component of reaction center-light harvesting 1 (RC–LH1) core complexes from several species in the *Rhodobacter* genus of purple photosynthetic bacteria, but many aspects of its structure and function are still poorly understood, and are the subject of debate [1]. For example there are differing reports of the solution structure of the PufX polypeptide from *Rhodobacter* (*Rba.*) *sphaeroides* in organic solvent, proposing either bent or linear secondary structures for its central α-helical domain extending between residues Asn13 and Met53 (numbering as in [1]). In the first of these, nuclear magnetic resonance (NMR) data yielded a bent helix that would allow the entire helical region to reside in the interior of the membrane or at its surface [2]. The C-terminal half of the helix was proposed be arranged perpendicular to the membrane plane and to extend most of the way across the span of the membrane. The N-terminal half was arranged at an angle of approximately 60° to the membrane plane, facilitated by a helix bend of around 120° [2]. A subsequent report presented an essentially linear structure for the central helix of PufX which, given its 41 amino acid length, would imply that one or both ends of the helix would extend significantly beyond the span of the membrane [3].

These contrasting interpretations of rather similar NMR data have had strongly differing effects on subsequent structural and modeling studies of the dimeric RC–LH1 complex from *Rba. sphaeroides*. An 8.5 Å resolution projection structure of the dimeric RC–LH1 complex, derived from cryo-electron microscopy of two-dimensional (2-D) crystals of this complex and single particle reconstruction studies [4,5], showed a strong electron density within the LH1 ring adjacent to the RC Q_B site. The transmembrane domain of the bent PufX structure [2] could be fitted into this density in such a manner that the long N-terminal domains of the two symmetrical PufX polypeptides within the dimer

Abbreviations: AFM, atomic force microscopy; EDTA, ethylenediamine tetraacetic acid; HEPES, *N*-2-Hydroxyethylpiperazine-*N*'-2-Ethanesulfonic Acid; HSQC, Heteronuclear single quantum coherence; ICM, intracytoplasmic membrane; LH1, light harvesting 1 complex; LH2, light harvesting 2 complex; MDFF, molecular dynamics flexible fitting; NMR, nuclear magnetic resonance; NOE, Nuclear Overhauser Effect; *Rba.*, *Rhodobacter*; RC, reaction center; RC–LH1, reaction center-light harvesting 1; SDS-PAGE, sodium dodecyl sulfate polyacrylamide gel electrophoresis; six-histidine, His_6, six–histidine; Tris, Tris(Hydroxymethyl)aminomethane; TROSY, Transverse Relaxation Optimised Spectroscopy; 2-D, two-dimensional; β-DDM, β-dodecylmaltoglucoside

* Corresponding author. Tel.: +44 114 222 4191; fax: +44 114 222 2711.
E-mail address: c.n.hunter@sheffield.ac.uk (C.N. Hunter).

0005-2728/$ – see front matter.
doi:10.1016/j.bbabio.2010.10.003

were able to extend along the cytoplasmic surface of the complex towards the dimer interface, enabling the N-terminus of PufX from one half of the dimer to make contact with surface-exposed groups from the other half. The implication of this model was that the two PufX N-termini could engage in a crosslinking arrangement that could promote or stabilise dimer formation [4]. This disposition of the N-terminus of PufX is a direct consequence of the bend in the membrane-spanning helix and predicts that progressive deletion of the N-terminus should affect dimerisation of the complex. Intriguingly, Francia et al. have shown that this is indeed the case, removal of the first seven residues from the N-terminus of PufX largely abolishing dimerisation of the RC–LH1 complex [6].

The solution NMR structure of PufX with a long, almost straight helix [3] lends itself to a different structural model for the RC–LH1 dimer in which the membrane-spanning helices of two PufX polypeptides interact directly at the dimer interface [7]. In such an arrangement, the sequence $G^{31}xxxG^{35}$ involving Gly31 and Gly35 would be available as a helix–helix dimerisation motif, as found in glycophorin A [8]. The $G^{31}xxxG^{35}$ sequence has been proposed to drive the dimerisation of the RC–LH1 core complex, a straight helical secondary structure for the PufX polypeptide allowing a close approach of the GxxxG motifs [7,9]. Recently, however, the glycine residues of the proposed $G^{31}xxxG^{35}$ dimerisation motif were mutated to leucine without affecting dimer assembly [10].

Another aspect of the *Rba. sphaeroides* PufX polypeptide which has produced some disagreement in the literature is whether or not the C-terminus is processed. The N-terminus of PufX is found on the cytoplasmic side of the intracytoplasmic membrane (ICM) [11]. The topology of the C-terminus has not been determined, but analysis of the *Rba. sphaeroides* PufX has shown that it consists of 83% hydrophobic and neutral residues, suggesting that it is an intrinsic membrane protein with an N_{in}–C_{out} orientation [12]. The mature PufX polypeptide has been reported to be 12 amino acids shorter than the DNA sequence predicts; two separate mass spectral analyses of the mature PufX gave similar values of 7576 Da and 7582 Da [13], smaller than the mass predicted by the gene sequence of 9052 Da [11]. The C-terminal amino acid was found to be alanine, consistent with the processing of 12 residues, which would give a predicted mass of 7575 Da [13]. An alternative view of C-terminal processing was suggested by the work of Francia and co-workers [14], who attached a six-histidine (His_6) sequence to the C-terminus of PufX. It was found that this His_6 tag was detected, implying a lack of C-terminal processing, this lack of correspondence with the results of Ref. [13] being suggested to arise from the use of different strains of *Rba. sphaeroides*, with both the LH1 and LH2 antenna complexes present in one case [14] and neither LH complex present in the other [13]. This implied that the presence of LH2 (or LH1) could influence the processing of PufX [6].

The work presented in the present paper attempts to resolve issues surrounding the structure of PufX and its C-terminal processing. New structural information for PufX has been obtained in a detergent micelle rather than organic solvent, as this provides a better mimic of the lipid bilayer environment, as already shown for the LH1 β polypeptide [15]. A bent conformation for the helix of PufX implies a particular function for residue Gly29, which is conserved in all known PufX sequences, and the validity of this is tested through site-directed mutagenesis. In addition, mutagenesis, biochemical methods and AFM are used to further analyse the effects of deletions at the N-terminus of PufX on the formation of RC–LH1 dimers. Finally we used His_6- and T7-tagged PufX constructs to revisit the issue of C-terminal processing of this polypeptide.

2. Materials and methods

2.1. NMR spectroscopy of purified PufX

For NMR studies, PufX was expressed using an autoinducing medium [16] as described previously [2], using ^{15}N ammonium sulfate as the nitrogen source and ^{13}C glycerol (2.5 g/l) as the carbon source. Purification was carried out as described [2,17,18]. Approximately 100 nmol of labeled protein was dissolved in methanol:chloroform (1:1 v:v), added to a solution of 40 mg Zwittergent 3-14 in the same solvent, and dried down with nitrogen gas. The dried mixture was dissolved in 50 mM potassium phosphate pH 6.

All NMR measurements were conducted at 37 °C, using a Bruker Avance 600 equipped with a cryoprobe. Backbone assignments were carried out using standard (non-Transverse Relaxation Optimised Spectroscopy (TROSY): TROSY experiments gave poorer signal-to-noise ratios) 2D and 3D experiments: HSQC (Heteronuclear single quantum coherence), HNCO, HN(CA)CO, CBCA(CO)NH, HNCACB, HNCA. Spectra were processed using Felix (Felix NMR Inc, San Diego, CA), and the assignment was carried out with the help of the program *asstools* [19].

2.2. Preparation of intracytoplasmic membranes

Rba. sphaeroides cultures were routinely grown in M22+ medium semi-aerobically in the dark at 30 °C, to induce maximal pigment synthesis [11,20]. Cultures were grown in 2-l conical flasks containing 1.6–l of growth medium, to an absorbance of 3.0 at 680 nm. Harvested cells were resuspended in 10 ml of membrane buffer (20 mM N-2-Hydroxyethylpiperazine-N'-2-Ethanesulfonic Acid (HEPES), 1 mM ethylenediamine tetraacetic acid (EDTA), pH 7.8), a few crystals of DNase I were added, and the cells disrupted in a French pressure cell at 18,000 p.s.i. The broken cells were centrifuged at 18,000*g* for 30 min to pellet cell wall material. The supernatant was layered onto a discontinuous (20/40% w/v) sucrose gradient, and the gradient centrifuged in a Beckman SW32 rotor at 89,500*g* for 10 h. The intracytoplasmic membrane (ICM) fraction formed a band above the 20/40% interface, and was collected using a peristaltic pump and stored at −20 °C until required.

2.3. Atomic force microscopy

ICM vesicles were opened out to form membrane patches suitable for high-resolution atomic force microscopy (AFM) by treatment with 0.02% (w/v) β-DDM and fractionated on a 20–45% (w/w) sucrose gradient containing 20 mM HEPES pH 7.5, 5 mM EDTA and 0.02% (w/v) β-dodecylmaltoglucoside (β-DDM) by centrifugation at 200,000*g* for 12 h in a Beckman SW41 rotor. The pigmented fraction at ~35% sucrose was recovered. The membranes were adsorbed onto freshly cleaved mica (Agar Scientific) in an adsorption buffer of 10 mM HEPES pH 7.5, 150 mM KCl, 25 mM $MgCl_2$ for 1–1.5 h. The sample was then gently washed with the imaging buffer (10 mM HEPES pH 7.5, 100 mM KCl).

All imaging was performed using a commercial Veeco Nanoscope IV AFM equipped with an 'E' scanner (15×15 μm), in Tapping Mode under imaging buffer. Sharpened silicon nitride cantilevers (Olympus TR800, $k = 0.15$ N m^{-1}) were used, in a standard Veeco tapping mode fluid cell, with drive frequency at 7–10 kHz. Images were recorded at 512×512 pixels, at scan frequencies of 0.5–1.5 Hz. Low tapping amplitudes were used and tip-sample interaction forces kept minimal by careful parameter optimisation. Images were processed and three-dimensional representations made using the Nanoscope (v6) software (Veeco).

2.4. Site-directed mutagenesis of PufX

Mutations of residue Gly29 were generated using the QuikChange method (Stratagene) using plasmid pUCXB-3 as the template [21]. Nucleotide changes were confined to the codon of Gly29 and were confirmed by DNA sequencing (Cogenics Inc.). Altered *pufX* genes were shuttled into the broad-host range vector pRKEH10, which is pRK415 containing a ~6.5 kb *Eco*RI–*Hin*dIII restriction fragment that

includes the *pufBALMX* operon. This was inserted into the *Rba. sphaeroides* strains DPF2 [22] or DD13 [23] through conjugative crossing [24]. Complementation of *puf* operon deletion strain DPF2 in this way gave transconjugant strains containing reaction centers (RCs), light harvesting 1 (LH1), PufX and light harvesting 2 (LH2) complexes, while complementation of double *puf/puc* operon strain DD13 gave transconjugant strains containing RCs, LH1, PufX but lacking LH2. Control strains comprised DPF2 or DD13 complemented with a version of the pRKEH10 plasmid either containing a wild-type copy of *pufX* or with a deletion of *pufX*. Strains were stored as glycerol stocks at −80 °C.

2.5. Construction of PufX mutants with truncations at the N-terminus

Altered versions of *pufX* with a shortened N-terminus were constructed by John Kirkland, University of Sheffield. Expression of the altered *pufX* genes in deletion strains DPF2 and DD13 was carried out as described for the Gly29 mutants above.

2.6. Construction of PufX mutants tagged at the N- or C-terminus

PufX was tagged at either the N- or C- terminus with a T7-tag (constructed by John Kirkland, University of Sheffield) or a His_6-tag (constructed by Dr. Rachel Pugh, University of Sheffield). The tagged *pufX* genes were cloned into the plasmid pRKEHXSB1, which contains the *puf* operon with *pufX* removed. The plasmids were then mated into *Rba. sphaeroides* deletion strains DD13 or DPF2 , as for the Gly29 mutants above. Mutant strains with a T7 tag at the N or C terminus of PufX were named NT7 or CT7, respectively, while strains with a His_6 tag at the N or C terminus of PufX were named $NHis_6$ or $CHis_6$, respectively.

2.7. Analysis of the monomer/dimer core complex content

ICM prepared using the method described above were pelleted by ultracentrifugation at 100,000*g* for 2.5 h and resuspended with gentle homogenisation in 20 mM HEPES buffer at pH 7.8 to an absorbance of 100 at 875 nm. Membranes were solubilised using β-DDM (Glycon Biochemicals, Germany) at a concentration of 3% w/v and incubated at 4 °C in the dark for 30 min with constant mixing. Insoluble material was removed by centrifugation at 171,500*g* for 60 min. 1.67 ml of supernatant was loaded onto a 20/25/30/35/40% w/w sucrose density step gradient prepared with 20 mM HEPES, 0.03% β-DDM, pH 7.8 and centrifuged for 40 h at 200,000*g* in a Beckman SW41 rotor. For mutants in the LH2-containing background the ICM were prepared using the same protocol but fractionation of the solubilised material involved using a 20/21.25/22.5/23.75/25%, w/w sucrose density step centrifuged at 100,000*g* for 40 h.

2.8. Assays of photosynthetic growth

All photosynthetic growth was monitored using strains expressing the LH2 antenna. Glass screw-cap test tubes containing M22+ media were sparged with nitrogen gas, then inoculated with cells taken from 80 ml semi-aerobic cultures. Any remaining oxygen was removed by incubating the tubes in the dark overnight. The volume of inoculum was calculated so that a final absorbance of 0.05 at 680 nm in a total volume of 13 ml was achieved. Tubes were placed in a temperature-controlled water bath exposed to a light intensity of 250 μmol m^{-2} s^{-1}. Growth of the cultures was monitored by measuring optical density at 680 nm using a colorimeter (WPA Colourwave C07000).

2.9. Timecourse of photosynthetic membrane assembly

The method used has been described previously [11], and was based on earlier work [20]. In outline, cells were first grown aerobically with a high oxygen tension, which inhibited the formation of photosynthetic membranes, then transferred to a flask for oxygen-limited, semi-aerobic growth to induce the production of pigmented intracytoplasmic membranes. At various time intervals a 1-ml sample of the culture was collected, the flask replenished with 1 ml of medium, and the absorbance spectrum of each sample was recorded (results not shown). Protease inhibitors (Roche Complete) and DNase were added before the sample was flash frozen in liquid nitrogen and then stored at −20 °C until ready for further analysis. Cell samples of both strains were collected at the following times after induction of photosynthetic membrane production: 0, 10, 20, 40 min, 1, 2, 4, 6, 8, 12, 22 h.

2.10. Western blot analysis

Protein samples were separated on discontinuous Tricine-sodium dodecyl sulfate polyacrylamide gel electrophoresis (SDS-PAGE) gels according to the method of Schägger and Von Jagow [25]. Samples of *Rba. sphaeroides* membrane proteins were incubated at 65 °C for 15 min in 2× Schägger gel sample loading buffer (2% SDS, 24% glycerol (w/v), 100 mM Tris(Hydroxymethyl)aminomethane (Tris), 4% mercaptoethanol (v/v), 0.02% bromophenol blue, adjusted to pH 6.8 with HCl), unless otherwise stated. The gels were run at 30 V for 1 h and then 90 V for approximately 4 h.

Western analysis was essentially performed as in Sambrook et al. [26]. Following western blotting, the nitrocellulose membrane was blocked for 60 min at room temperature in 50 ml blocking reagent (10 mM Tris–HCl pH 7.5, 150 mM NaCl, 5% milk powder, 0.05% Tween-20) with shaking. The membrane was then incubated with the primary antibody in 25 ml blocking reagent for 60 min at room temperature with shaking. The membrane was washed with western wash buffer (10 mM Tris–HCl pH 7.5, 150 mM NaCl) for 2 × 1 min, and then incubated with the secondary antibody in 5 ml blocking solution for 60 min at room temperature with shaking. Finally, the membrane was washed for 3 × 10 min in western wash buffer. Immunodetection was performed using enhanced chemiluminescence detection reagents supplied by Amersham (ECL Detection System) according to the manufacturer's instructions. Almost all primary antibodies were used in a 1:5000 dilution in blocking solution, and detected using horseradish peroxidase-conjugated goat anti-rabbit antisera, at a 1:5000 dilution, as the secondary antibody. The exception was anti-His_6 antibodies that were raised in mice so detection was carried out using horseradish peroxidase-conjugated rabbit anti-mouse antiserum.

3. Results

3.1. Structural analysis of PufX in a detergent micelle

In order to obtain new structural information on PufX, the protein was solubilised in detergent micelles rather than the methanol/chloroform organic solvent used in previous studies [2,3], taking the view that micelles are a better approximation of a biological membrane than organic solvents. Preliminary studies showed that the most suitable detergent for maintaining PufX in solution was Zwittergent 3-14, and that the best temperature was 37 °C. However, even under these optimised conditions, micellar samples of PufX were not sufficiently well behaved to allow measurements of NOE spectra for detailed structure calculations; many of the signals from PufX were broad and/or split, and the sample only lasted approximately 2 weeks before precipitating irreversibly. Structural analyses were therefore based on relaxation effects, which are governed by local mobility and therefore provide information on the regions of the protein that maintain a defined conformation. The intensities of signals in 3D NMR spectra depend mainly on their T_1 and T_2 relaxation rates, which exert their effects through loss of magnetization during

the pulse sequence and by broadening the signal; the T_2 rate exerts more influence because this is the shorter relaxation time [27]. Relaxation rates depend mainly on the mobility of the atoms involved. For a peptide in a micelle, two different relaxation regimes can be observed: within the micelle, the amino acids tumble slowly and therefore have low signal intensities, whereas amino acids outside the micelle tumble much more rapidly and have high intensities.

It was not possible to measure T_2 data directly for PufX in micelles, because the spectra were of poor quality and the sample was not stable enough for extended measurements. A proxy measurement for T_2 was therefore used, namely the intensity of the 3D HNCA signal, which is related to the T_2 time. The intensities in the HNCA spectrum, shown in Fig. 1A, were markedly lower for residues 17–54, implying that these residues are inside the micelle, and only able to tumble slowly. In contrast, the higher intensities for many of the residues in the regions 2–16 and 58–80 indicated that residues at the N- and C-termini of the protein are significantly more mobile. For comparison, Fig. 1A also shows T_2 relaxation data measured for PufX in methanol/chloroform [2], which generally parallel the HNCA intensities, strongly suggesting that the overall helix–turn–helix conformation seen in methanol/chloroform is maintained in micelles. In particular, the comparison shows that residues 17–54, previously assigned to a helical region in organic solvent, are also constrained within the micelle. The N-terminus (residues 1–16) and C-terminus (residues 58–80) are predicted to lie outside the micelle.

In order to check whether these conclusions were consistent with the size of the Zwittergent 3-14 micelles, we calculated the micelle dimensions on the basis of published data [28]. These calculations showed that a typical micelle is expected to contain approximately 130 detergent molecules and to be approximately 33.4 Å radius along the long axis and 20.2 Å radius along the short axis (to the center of the headgroups). The overall structure of PufX determined in organic solvent [2] fitted well within the dimensions of a typical micelle, shown in Fig. 1B using red spheres for the zwitterionic headgroups. This conclusion was consistent with the predictions from HNCA intensities shown in Fig. 1A. Since, in principle, only 23 amino acids are necessary to span a membrane as an α-helix, the only way to constrain the mobility of the 38-residue sequence (residues 17–54, inclusive), represented by the pale blue box in Fig. 1A, is to invoke a bend in the PufX α-helix with the N-terminal half of the helix associated with the micelle surface. The darker box in Fig. 1 shows the transmembrane region of 21 residues between Phe24 and Ile44 proposed by [3], which is much shorter than the region of low HNCA intensity in our data. In the linear model for PufX, residues 13–23 and 45–53 at either end of the helix would be expected to lie outside the proposed transmembrane region, to exhibit more mobility and therefore show more intense HNCA signals, but this was not observed in our data. Thus, the helix–bend–helix structure of PufX determined in organic solvents [2] is much more compatible with the micelle-derived NMR data, and fits well into the expected dimensions of the micelles used as a membrane mimic.

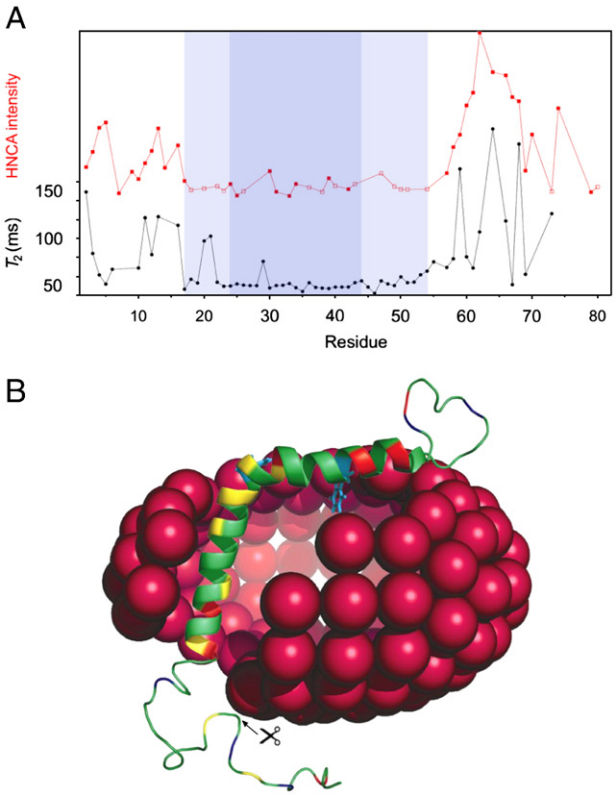

Fig. 1. Comparison of NMR data for PufX in methanol/chloroform and embedded in Zwittergent 3-14 micelles. (A) Signal intensity in the 3-D HNCA spectrum plotted *versus* sequence position, shown as filled red squares for residues with a high confidence of assignment (i.e., a full set of matches in triple resonance spectra), and as open squares where there is a lower degree of confidence for the assignment. The intensity units are arbitrary. For comparison, T_2 relaxation data for PufX in methanol/chloroform [2] are shown in black. The pale blue box corresponds to residues 17–54, previously assigned to a helical region in organic solvent, which are also constrained within the micelle. The N-terminus (residues 1–16) and C-terminus (residues 58–80) are predicted to lie outside the micelle. The darker blue box shows, for comparison, the highly conserved α-helical region composed of 21 residues (Phe24-Ile44) assigned in ref [3]. (B) One of the NMR-derived structures for PufX in methanol/chloroform [2]. The positions of the two tryptophan residues (which are often used as markers for the bilayer boundary: [65] are indicated in pale blue; glycines are in yellow, basic residues in crimson red and acidic residues in dark blue. Approximate dimensions of the Zwittergent 3-14 micelle are indicated by the ellipse, with the red spheres representing the zwitterionic headgroups. Selected headgroups have been removed to indicate how the PufX polypeptide could be located within a micelle approximately 33.4 Å radius along the long axis and 20.2 Å radius along the short axis. For comparison, the hydrophobic portion of a typical membrane bilayer is approximately 30 Å across. The location of C-terminal processing is indicated.

3.2. Mutagenesis of the conserved residue Gly29

A striking feature of the five published sequences of PufX from different species of *Rhodobacter* is the low degree of sequence identity displayed (see discussion in Ref. [1]). An alignment of these sequences, first published by Tsukatani and co-workers [29], is reproduced in Fig. 2A. Only eight residues (highlighted in red) are absolutely conserved between these sequences. Of particular interest in the context of the present report is the absolutely conserved Gly at position 29, which is located on the inside of the bend in the structure of PufX shown in Fig. 1B. The position of this Gly and its conserved nature could suggest that the bend is facilitated by a very small amino acid at this crucial location, and further that a helix–bend–helix architecture is common to the PufX proteins of the five species listed in Fig. 2A.

To test this hypothesis Gly29 was mutated to Ala, Val, Ile and Leu; i.e. to progressively larger hydrophobic sidechains. Strains were constructed either possessing or lacking the LH2 antenna protein. All mutants were grown under dark/semi-aerobic conditions and purified ICM were prepared and solubilised in β-dodecylmaltoglucoside (β-DDM) as described in Materials and Methods. Fig. 2B shows the effect of these mutations on dimer formation in semiaerobically grown cells lacking LH2 complexes, assessed through detergent extraction and sucrose gradient fractionation; LH2 ran at the top of the gradient, and the remaining upper and lower bands represented monomer and dimer core complexes respectively. The normal dimer population in the PufX-containing control strain PufX$^+$ (extreme left) was reduced when Ala was present at position 29 (G29A, extreme right), and was abolished by Val, Ile and Leu mutations. The western blots in Fig. 2C show that this loss of dimer coincides with a major decrease in the amount of PufX in

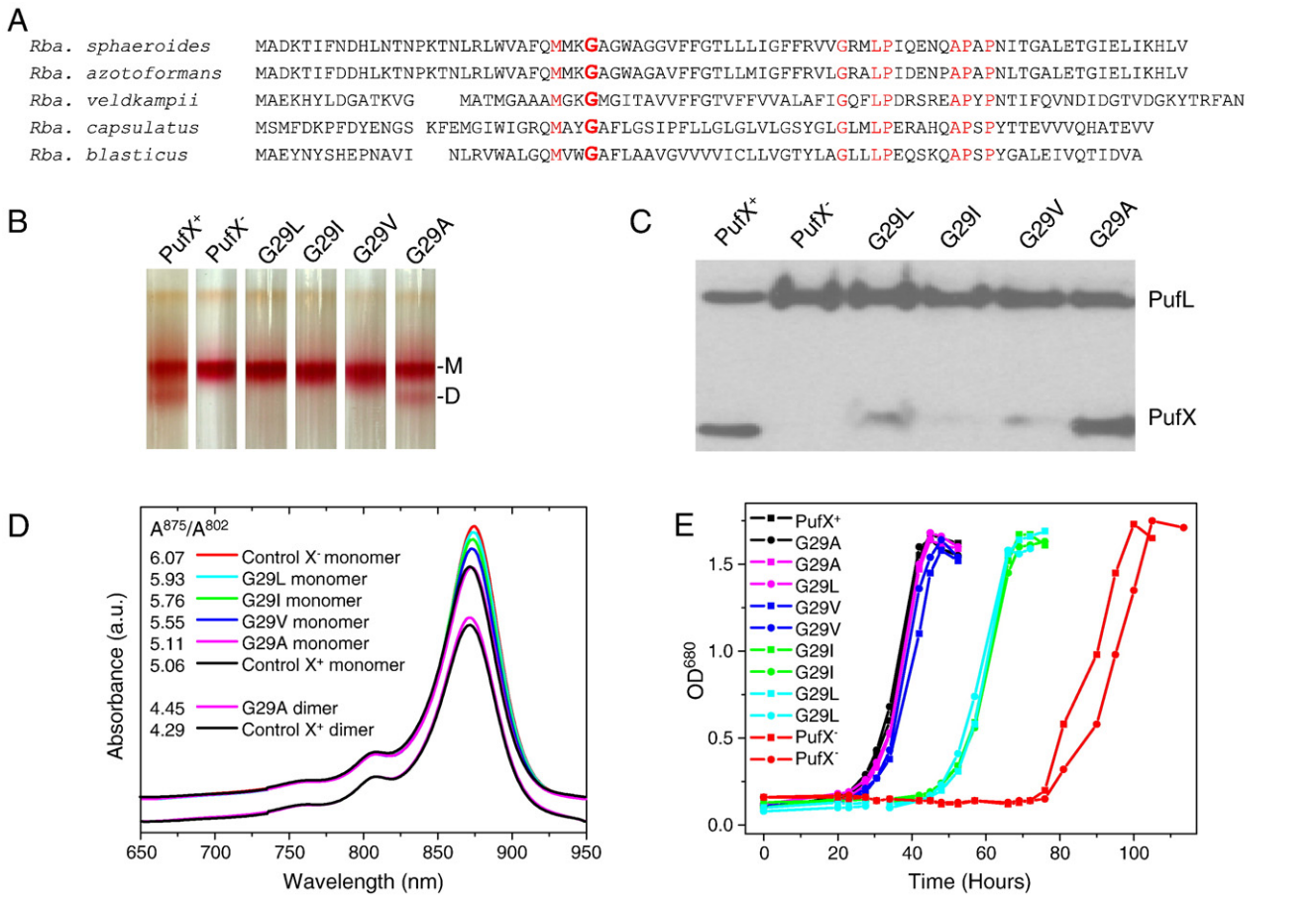

Fig. 2. Consequences of mutation of the conserved Gly29 to Ala, Val, Ile or Leu. (A) Alignment of PufX homologs, as originally presented by Tsukatani et al. [29]. The conserved Gly29 is shown in bold red typeface; other conserved residues are shown in red. (B) Sucrose gradients of monomeric and dimeric RC–LH1 complexes extracted from strains lacking the LH2 antenna. M-core monomer; D-core dimer. (C) Western blot analysis of proteins extracted from membranes of the PufX Gly29 mutants, probed with anti-PufX and anti-PufL antibodies; PufL is a component polypeptide of the RC used as a loading control. (D) Absorbance spectra of fractions from the pigmented bands in the sucrose gradients shown in (B). Raw spectra were corrected for background scatter between 650 and 950 nm and normalised to the same absorbance at 802 nm. The spectra of the dimeric complexes have been displaced vertically for clarity. Numbers in the inset legend refer to the ratio of (mainly) LH1 absorbance at 875 nm to (mainly) RC absorbance at 802 nm. (E) Effect of mutation of Gly29 on photosynthetic growth, tested in strains that possess the LH2 antenna. Cultures were grown in pairs.

the membrane, which could mean that Gly29 is essential for the stable incorporation of PufX into the membrane/core complex. Fig. 2D shows the effects of the mutations on the absorbance spectrum of the monomeric and, where present, dimeric forms of the core complex. In addition to the spectra, the ratio of (mainly) LH1 absorbance at 875 nm to (mainly) RC absorbance at 802 nm is presented. Consistent with previous reports, monomeric RC–LH1 complexes from strain PufX$^-$ had a higher A_{875}/A_{802} than those from the PufX$^+$ strain , explained by loss of PufX allowing a complete $(\alpha\beta)_{16}$ LH1 ring to encircle the RC (Fig. 2D). In the Gly29 mutants, the A_{875}/A_{802} ratio was little changed in the Ala mutant, but showed progressive increases in the Val, Ile and Leu mutant to a value approaching that of the PufX$^-$ control (Fig. 2D). Similar data were obtained from an equivalent set of strains also containing LH2 (not shown). Taken together, the data in Fig. 2C and D indicated that the G29V, G29I and G29L mutants had a mixed population of PufX-containing and PufX-deficient monomeric core complexes, the relative amount of the latter being the greatest in the G29I and G29L strains.

The effects of the Gly29 mutations on photosynthetic growth were also recorded, using the strains also expressing the LH2 antenna. The PufX$^+$ control exhibited a highly reproducible lag of around 20 h before the onset of photosynthetic growth. This lag represents an adaptation from semiaerobic/dark to photosynthetic growth conditions, and has been reported previously for similar PufX-containing strains [34,35]. The G29A and G29V mutations exhibited similar photosynthetic growth whereas the PufX$^-$ control commenced growth only after a lag of approximately 70 h (Fig. 2E). These data were in line with the longstanding observation that PufX is essential for normal photosynthetic growth [30–33]. Strains with the G29I and G29L mutations presented interesting intermediate cases where there was growth after an intermediate lag period, possibly due to the traces of PufX seen in the western blots, which allows a sub-population of active photosynthetically-competent PufX-containing cores to assemble. The nature of the adaptive lag before the onset of photosynthetic growth is the subject of ongoing investigation, but it is unlikely to represent a period required to remove residual oxygen from the photosynthetic cultures, as this would not be expected to be sensitive to point mutations in PufX, and to be longer for the G29I or G29L mutants. Also, for the PufX$^+$ strain the ~20 h length of the lag was not altered by a period of dark preincubation of the photosynthetic cultures of up to 20 h (i.e. the 20 h adaptation from semiaerobic/dark to photosynthetic growth conditions only began once the cultures were exposed to light (Crouch, L.I and Jones, M.R., unpublished observations)). Preliminary studies indicate that the precise length of the lag is dependent on the presence or absence of the LH2 antenna, being longer in its absence, and on the intensity of illumination, being longer at lower light intensities (Crouch, L.I and Jones, M.R., unpublished observations). This suggests that the processes

occurring during this lag phase are dependent on the activity of the photosynthetic apparatus, which would explain why the lag is longer in strains such as G29I and G29L which contain a significant proportion of photosynthetically-incompetent, PufX-deficient core complexes.

In summary, therefore, increasing the volume of the residue at position 29 beyond Ala reduced the amount of PufX in the membrane, reduced or abolished the formation of RC–LH1 dimers, increased the LH1 content of monomeric RC–LH1 complexes and delayed the onset of photosynthetic growth, the strength of the recorded effects tending to increase in the order A<V<I/L.

3.3. The structural role of the N-terminus of PufX: the effects of PufX N-terminal truncations on the dimerisation of core complexes

The structure of PufX in Fig. 1B predicts that the N-terminal region of PufX will lie along the cytoplasmic face of the membrane. Before any structural data were available, Francia et al. [6] progressively deleted 3, 6, 18 or 25 residues from the N-terminus of the *Rba. sphaeroides* PufX (excluding the N-terminal Met) and showed that the first 7 residues at the N-terminus strongly influenced dimerisation of core complexes. The mutant lacking 6 residues at the N-terminus showed strongly decreased amounts of dimeric RC–LH1 complex, as assessed by sucrose gradient fractionation of detergent-solubilised complexes, while removal of the 18 N-terminal residues completely abolished the formation of core complex dimers. In the light of subsequent structural information, the loss of 18 amino acids would involve removal of the N-terminal end of the long, bent PufX helix. The work in the present report attempted firstly to narrow down the point at which truncation of the N-terminus causes the complete loss of dimeric core complexes. Second, we analysed the amounts of monomer and dimer in one of the N-terminal deletion mutants through a technique that does not require detergent solubilisation, using AFM to directly visualise the aggregation state of core complexes in intact membranes.

A nested series of 6 N-terminal truncation mutants of PufX (ΔN-3, ΔN-7, ΔN-12, ΔN-18, ΔN-28, ΔN-32; see Fig. 3A and B) was used to establish the minimal PufX structure necessary to sustain dimerisation of RC–LH1–PufX cores. As above, experiments were carried out in strains both possessing and lacking the native LH2 antenna. Fig. 3C shows an analysis of the aggregation state of core complexes in strains possessing LH2, as assessed through fractionation of DDM-solubilised pigment-proteins on sucrose density gradients. In the PufX$^+$ control (lane 1) approximately half of the RC–LH1–PufX core complexes were in the dimeric state, whereas only the upper monomer band was present in the PufX-deficient control (lane 2). As in the PufX$^+$ control, a dimer band was present in the ΔN-3 truncation mutant, although a trend towards increasing monomer content at the expense of the dimer population was noticeable, particularly in the ΔN-7 mutant. Truncation of 12 or more residues from the N-terminus resulted in the complete loss of a dimer band (Fig. 3C, lanes 5–8). Western blot analysis of the starting membranes was used to distinguish between the direct effect of truncation on core dimerisation and an indirect

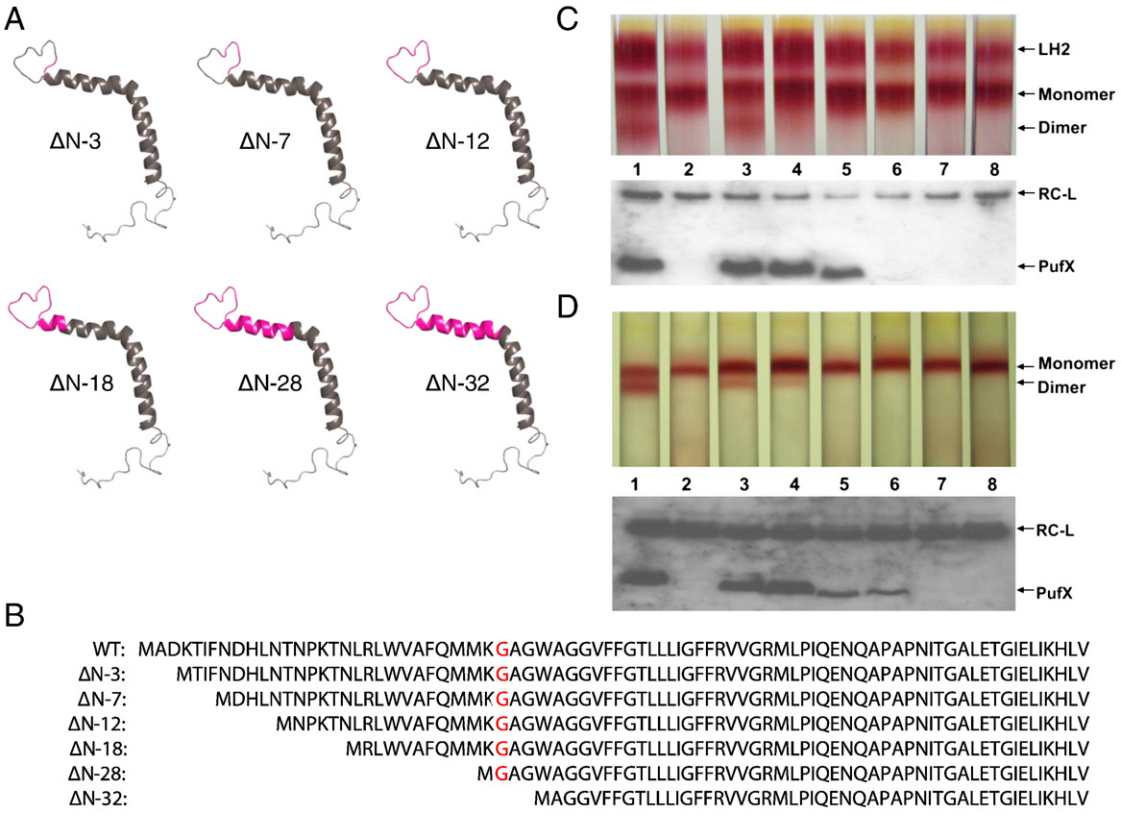

Fig. 3. Analysis of N-terminal deletion mutants of PufX. (A) Cartoon representation of the PufX polypeptide and the N-terminal deletions. The regions removed by the N-terminal truncations are indicated in magenta. (B) Sequences of the PufX polypeptides represented in (A) and analysed in (C) and (D). Gly29 is highlighted in red. (C) Discontinuous sucrose gradients and western blots of pigment proteins extracted from *Rba. sphaeroides* strains containing LH2 and expressing N-terminal truncations of PufX. The gradients show bands arising from detergent-solubilised pigment proteins, with LH2 complexes uppermost, then core monomers then dimers lowest in the gradient. Western blots on proteins isolated from ICM and separated by PAGE were carried out using antibodies to the RC–L subunit as a loading control and also probed with antibodies to PufX. The samples are derived from strains: 1. PufX$^+$, 2. PufX$^-$, 3. ΔN-3, 4. ΔN-7, 5. ΔN-12, 6. ΔN-18, 7.ΔN-28, 8. ΔN-32. (D) Discontinuous sucrose gradients and western blots of pigment proteins extracted from *Rba. sphaeroides* strain lacking LH2 and expressing N-terminal truncations of PufX. The gradients show bands corresponding to core monomers (upper band) and dimers (lower band). Western blots were carried out as for (C). The samples are derived from strains: 1. PufX$^+$, 2. PufX$^-$, 3. ΔN-3, 4. ΔN-7, 5. ΔN-12, 6. ΔN-18, 7.ΔN-28, 8. ΔN-32.

effect arising from abolished assembly of PufX. The signal from immunodetection of the RC–L subunit was used as a loading control. The blots showed the expected absence of PufX from the PufX$^-$ control (Fig. 3C, lane 2), and also showed that the ΔN-3 and ΔN-7 mutants still possessed near-wild-type levels of PufX. Therefore, the significant loss of dimers in the ΔN-7 mutant was a specific effect of deleting the N-terminal sequence ADKTIFN. Additional deletion of residues DHLNT in the ΔN-12 mutant diminished dimer formation still further despite the presence of appreciable amounts of PufX. In the ΔN-18, ΔN-28 and ΔN-32 mutants, PufX was absent from the membrane, and only monomeric RC–LH1 complexes were isolated. The same series of N-terminal PufX deletion mutants was also analysed in a genetic background lacking LH2 complexes (Fig. 3D). Trends similar to those in Fig. 3C were observed, with the exception that mutant ΔN-18 contained a clearly detectable small amount of PufX, whereas in the LH2-containing background in Fig. 3C PufX was almost completely absent. This difference aside, both in the presence and absence of LH2 the dimeric form of the RC–LH1 complex was lost after removal of the N-terminal sequence ADKTIFNDHLNT.

The effects of the PufX N-terminal deletions on photosynthetic growth were assessed in the strains which contained the LH2 antenna (see Materials and Methods). Whereas the PufX$^+$ control grew rapidly after a lag of approximately 20 h, the truncation mutants lacking PufX, namely ΔN-18, ΔN-28 and ΔN-32, only grew after a lag of approximately 70 h, matching the PufX$^-$ control (not shown). The ΔN-3, ΔN-7 and ΔN-12 mutants showed some modest impairment of photosynthetic growth (not shown). These data showed that mutant ΔN-12, which retains PufX but lacks RC–LH1 dimers, had not lost the ability to photosynthesise. This reinforces the point that there is no direct link between the dimeric form of the RC–LH1 complex and the ability to grow under photosynthetic conditions [6].

3.4. Analysis of membrane organisation in mutants with N-terminal truncations in PufX

The data in Fig. 3C and D revealed differences in the relative amounts of detergent-solubilised dimeric and monomeric RC–LH1 complexes in the PufX truncation mutants. Atomic force microscopy was used to assess the effect of N-terminal truncation on organisation of RC–LH1 complexes in the membrane, to check whether the monomer/dimer compositions implied by the sucrose gradient analyses on detergent-solubilised complexes in Fig. 3 really reflect the situation in the membrane. Previous studies with different types of bacterial photosynthetic membrane have shown that AFM can distinguish between several types of organisation of complexes (for example, [36,37]; reviewed in [38]).

Fig. 4 shows high resolution AFM topographs of patches of membrane prepared from LH2-containing cells grown semi-aerobically in the dark, to aid comparison with the samples in the detergent/sucrose gradient experiment in Fig. 3C. Panel A shows the PufX$^+$ control, panel B a membrane patch from the PufX$^-$ mutant and panel C the ΔN-12 mutant. As expected from previously published AFM topographs on membranes from photosynthetically grown cells [37], membranes from the PufX$^+$ control showed rows of core dimers, delineated in red in Fig. 4A, with smaller rings of LH2 complexes situated on either side. The white areas are regions which had retained their high degree of native curvature and had not flattened onto the mica substrate sufficiently for imaging. In this patch we observed mainly core dimers, but the resolution did not permit an assignment of every core complex present. Nevertheless, in this patch there was no evidence for the substantial proportion of core monomers implied by the data in Fig. 2C, lane 1. More core monomers were seen in other patches (not shown), but dimers always formed a large proportion of the cores present. In contrast, membranes from the PufX$^-$ mutant showed a completely different organisation of complexes (Fig. 4B), with monomeric core complexes sometimes forming small clusters, but with no hint of the regular rows of dimers seen in Fig. 4A. To check that there were no dimers present, we measured the average distance between neighbouring RC–H subunits, seen in all three panels as the brightest features because these are the proteins at the greatest height above the mica surface. In the dimeric RC–LH1 complexes in Fig. 4A this distance was 7.8 nm, but in the image in panel 4B the closest approach of the high point of two RC–H subunits was 12 nm, indicating that, as also suggested by the data in Fig. 3, the core complexes in the membranes from the PufX$^-$ mutant consisted solely of monomers. A similar analysis of the image shown in Fig. 4C, recorded on membranes from a strain with the ΔN-12 mutation, likewise showed no evidence of core dimers. It was therefore concluded that the removal of residues ADKTIFNDHLNT in the ΔN-12 mutant does indeed abolish dimer formation, and that the detergent extraction/sucrose gradient fractionation approach in Fig. 3 is a useful method for assessing the monomer/dimer status of these mutants.

3.5. Processing of the PufX polypeptide at the C-terminus

The structural data obtained on the micelle-bound PufX polypeptide (Fig. 1) emphasized the exposure of the C-terminal domain, from Leu54 onwards, to the periplasmic compartment and therefore its potential availability for processing. As outlined above, previous attempts to determine if the C-terminus of PufX is processed produced conflicting data, potential complications arising from the

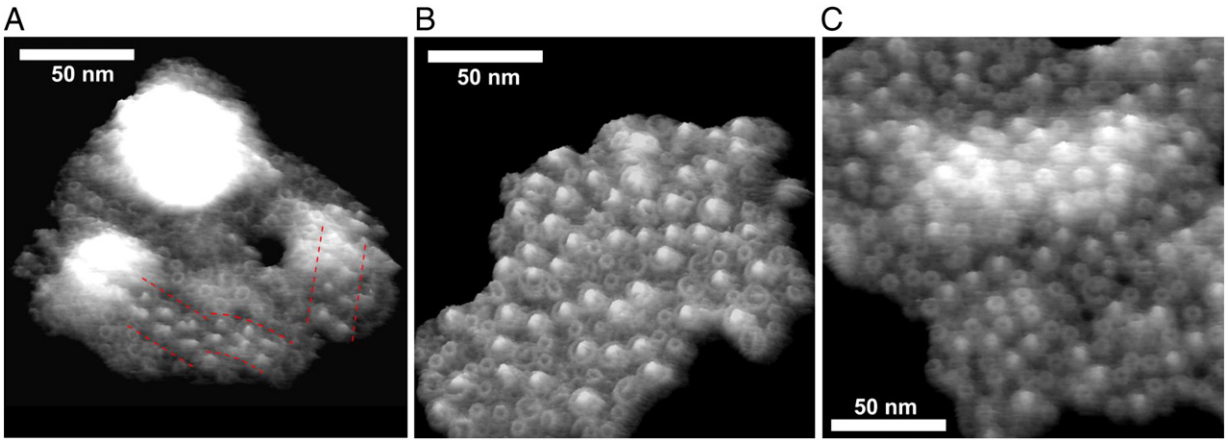

Fig. 4. The effect of a 12-residue truncation of the N-terminus of PufX on membrane organization probed by atomic force microscopy AFM topographs of membrane patches derived from strains containing LH2 complexes. (A) Control membrane patch from a pseudo-WT PufX$^+$ strain which assembles mainly dimeric core complexes. (B) A membrane patch from a mutant which has no PufX and assembles monomeric core complexes, (C) A membrane patch from mutant ΔN-12 which has a 12-residue deletion of the PufX N-terminal domain.

possible influence of a His_6 tag, whether purified polypeptides were being analysed, and the use of strains with or without LH complexes [6,13,14]. In the present work this problem was readdressed using two different tags, T7 or His_6, applied to either the N- or C-terminus, in strains with or without LH2. In addition, whole cells were also probed to avoid any potential problems with non-specific proteolysis during membrane or protein preparation. Absorption spectra of N- and C-terminally tagged strains (not shown) established that the tagging of PufX at either terminus with either T7 or His_6 had no discernable effect on dark/semi-aerobic growth of the cells or the assembly of intracytoplasmic membranes.

Membrane samples from each strain, along with the appropriate controls, were analysed using western blots (Fig. 5A–D). Fig. 5A shows the blot of separated proteins probed with anti-LH1α/PufX antibodies. All of the samples contained PufX, except for the negative controls DD13 ($LH2^-LH1^-RC^-PufX^-$; lane 7) and DPF2 ($LH2^+LH1^-RC^-PufX^-$; lane 8) both of which have a deletion of the *puf* operon. The PufX polypeptide with the N-terminal T7 tag ($LH2^-$, lane 1; $LH2^+$, lane 3) had a slightly higher molecular mass compared to the wild-type PufX in the complemented LH2–deficient and LH2–containing strains, and *Rba. sphaeroides* WT strain NCIB 8253, in lanes 5, 6 and 9, respectively. This suggests that PufX in the NT7 strains has retained the T7-tag at the N-terminus. In contrast, the PufX polypeptide tagged at the C-terminus with T7 (lanes 2 and 4) migrated to the same position as the native PufX protein, suggesting that the T7-tag was no longer present. To confirm the presence and absence of the T7 tag the nitrocellulose membrane was stripped and then reprobed with anti-T7-tag antibodies (Fig. 5C). The only samples that bound these antibodies were the NT7 stains without or with LH2 (lanes 1 and 3, respectively), confirming the absence of the T7-tag from the C-terminus of PufX in both the LH2-deficient strain (lane 2) and the LH2-containing strain (lane 4).

To further support the premise that PufX is processed at the C-terminus the same experiment was conducted with an N- or C-terminal His_6-tag. Fig. 5B shows the membrane samples probed with anti-LH1α/PufX antibodies; all the membrane samples contained PufX except for the negative controls in lanes 7 and 8. The results differed slightly from those with the T7 tag in Fig. 5A and C; PufX from $NHis_6$ strains without or with LH2 (lanes 1 and 3, respectively) had a higher molecular mass compared to the native PufX (lanes 6, 7 and 9) but there appeared to be some PufX polypeptide in lanes 1 and 3 migrating at the same molecular weight as the native PufX, suggesting that not all of the PufX polypeptide present was tagged. PufX from $CHis_6$ strains (lanes 2 and 4) migrated through the gel to the same position as native PufX, signifying that the His_6-tag was no longer present. Care was taken to load equal amounts of LH1 complex for each sample, and there appeared to be less PufX in the LH2-containing $CHis_6$ strain (lane 4) compared to the other strains that contain PufX. To confirm the presence of the His_6-tag the western blot was reprobed with antibodies to this tag (Fig. 5D). Apart from small signals from unspecific binding, the only two samples that gave a clear signal were those with the $NHis_6$-tag (lanes 1 and 3).

In order to eliminate non-specific proteolysis as the cause of the apparent C-terminal processing, an experiment was designed in which whole cells were rapidly removed from a culture and analysed by western blotting, avoiding the preparation of membranes required for the experiments shown in Fig. 5. Moreover, to check whether the processing might occur at a particular stage of photosynthetic development, cells undergoing a shift from an initially highly aerobic unpigmented state to an oxygen-limited fully pigmented one were analysed. This 22-h time-course of pigmentation allows for the possibility of detecting the C-terminal T7-tag on PufX during early stages of photosynthetic membrane assembly. Cell samples of strains NT7 and CT7, both with LH2 present, were harvested at various stages of this time-course, plus the appropriate positive and negative controls, then analysed by probing western blots with antibodies to either PufX or the T7 tag (Fig. 6). The anti-PufX antibodies did not detect a signal in cells with the N-terminal PufX tag until 2 h following the transition to low-aeration conditions that induced assembly of the photosynthetic membrane [11,20]. The signal intensities increased up to the 22-h timepoint in lane 11. Lanes 12, 13 and 14 are controls, with membranes from NT7, CT7 strains and an untagged strain, respectively (Fig. 6A). The anti-T7 antibodies followed the same trend, with increasing amounts of N-terminally tagged PufX in the pigmenting cells. In fact, the T7 antibodies were more effective than the PufX antibodies, and they elicited a stronger signal at the earlier timepoints (Fig. 6A). Thus, it is all the more significant that there was no signal in any of the timepoints with a C-terminal T7 tag on PufX (Fig. 6B); only the NT7 positive control in lane 12 had a positive reaction to the anti-T7 antibodies, so it appears that the PufX C-terminus is processed, even at the earliest stages of membrane assembly. To check for the presence of PufX in the cell samples from the CT7 time course experiment the nitrocellulose membrane was stripped and reprobed with anti-PufX antibodies. In lanes 7–11 where the anti-T7 antibody gives no signal, PufX could be detected using anti-PufX antibodies.

4. Discussion

In *Rhodobacter* species such as *sphaeroides* and *capsulatus* the PufX polypeptide is important for the architecture and function of the RC–LH1 core complex [1,39]. The lack of high-resolution structures of bacterial core complexes has hampered detailed analysis of the function of PufX, and there are conflicting reports in the literature regarding the structure, location and post-translational processing of this polypeptide. Given that *Rba. sphaeroides* is an important model organism for photosynthetic studies, and that counterparts of PufX might play roles in quinone gating in Photosystem II (reviewed in [1]) we have carried out further characterisation of the structure of PufX.

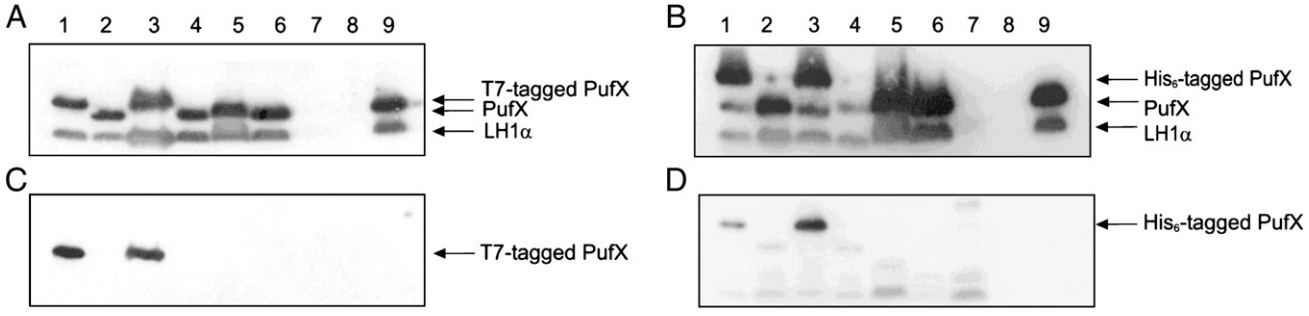

Fig. 5. Processing of PufX at the C-terminus analysed using western blots of constructs with a T7 or a His_6 tag. (A) Proteins were prepared from strains tagged either at the N- or C-terminus with the T7 sequence, and either lacking LH2 (lanes 1, 2, 5, 7) or containing LH2 (lanes 3, 4, 6, 8, 9). Lane 1. NT7; 2. CT7; 3. NT7 ($LH2^+$); 4. CT7 ($LH2^+$); 5. $PufX^+$; 6. $PufX^+$ ($LH2^+$); 7. DD13; 8. DPF2; 9. NCIB8253. The blot was probed with anti-LH1α and PufX antibodies. (B) Proteins were prepared from strains tagged either at the N- or C-terminus with the His_6 sequence, and either lacking LH2 (lanes 1, 2, 5, 7) or containing LH2 (lanes 3, 4, 6, 8, 9). Lane 1. $NHis_6$; 2. $CHis_6$; 3. $NHis_6$ ($LH2^+$); 4. $CHis_6$ ($LH2^+$); 5. $PufX^+$; 6. $PufX^+$ ($LH2^+$); 7. DD13; 8; DPF2; 9. NCIB8253. The blot was probed with anti-LH1α and PufX antibodies. (C) As (A) but probed with anti-T7 antibodies. (D) As (B) but probed with anti-His_6 antibodies.

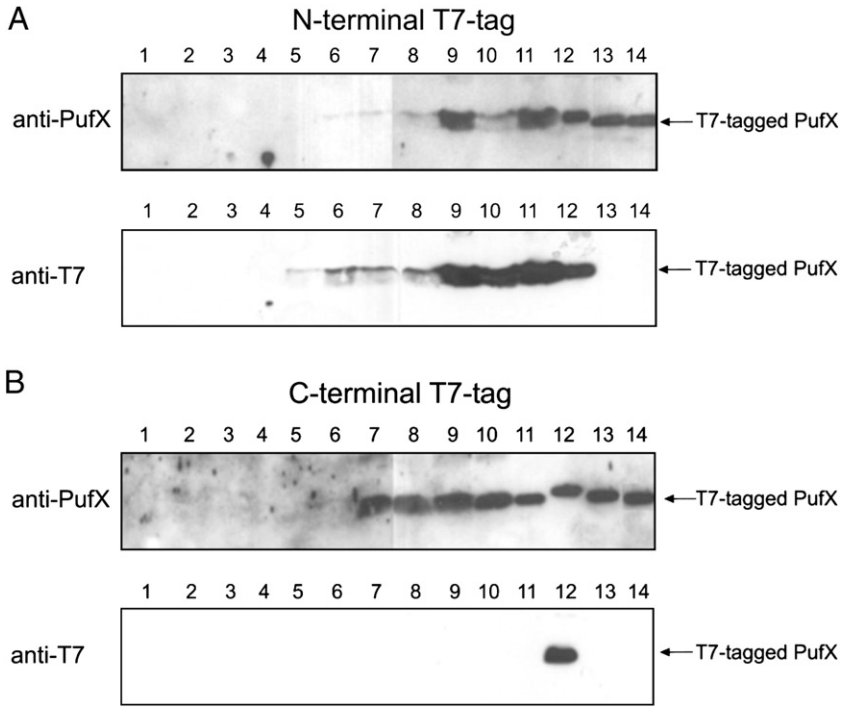

Fig. 6. Time-course of photosynthetic membrane assembly following the fate of N- and C-terminal T7 tags on PufX. Whole cell samples were removed from cultures induced for assembly of the photosynthetic apparatus, under semiaerobic conditions in the dark. The *Rba. sphaeroides* strains used for the time-course both had the capacity to assemble core and LH2 complexes, but contained PufX tagged with the T7 sequence at either (A) the N-terminus or (B) the C-terminus. Both western blots were probed with antibodies to either the T7-tag or PufX where indicated. The samples in the gel lanes are as follows: Lane 1, photosynthetic apparatus induced for 0 min; lane 2. 10 min; lane 3. 20 min; lane 4. 40 min; lane 5. 1 hr; lane 6. 2 hr; lane 7. 4 hr; lane 8. 6 hr; lane 9. 8 h; lane 10. 12 hr; lane 11. 22 hr; lane 12. control membranes of core complexes with the NT7 tag; lane 13. control membranes of core complexes with the CT7 tag; 14. control membranes of core complexes with no tag on PufX.

As outlined above, two structural models have been published for the *Rba. sphaeroides* PufX, one of which has a straight α-helix that would protrude significantly from either side of the membrane [3], and one in which the entire α-helix could be accommodated within the membrane, or at its surface, through a ~120° bend near the middle [2]. Two proposals have also been made as to the location of the PufX helix in the structure of the dimeric RC–LH1 complex. One places the membrane-spanning α-helices of two PufX polypeptides adjacent to one other at the dimer interface [40], while the alternative, based on an assignment from an 8.5 Å resolution projection map [4], places the α-helix of each PufX approximately 50 Å from the dimer interface, sandwiched between the surface of the RC and the surrounding LH1 antenna [4,5].

First, in support of the proposal that the PufX helices are at the dimer interface, it has been suggested that the sequence $G^{31}WAGG^{35}$ promotes dimerisation of the helices of two *Rba. sphaeroides* PufX proteins at this interface [40,41], through the type of GxxxG helix–helix dimerisation motif first characterised in glycophorin A [8]. This interaction has been modeled *in silico* using the straight PufX structure, and it has been proposed that the dimerisation of the membrane-spanning helices of PufX through the GxxxG motif seeds the formation of the entire RC–LH1 dimer [7,9] . However, the bent PufX structure supported by the data in the present publication would be incompatible with such an interaction, and it has also recently been shown that site-directed mutagenesis of neither Gly31 nor Gly35 to Leu affects the ability of the RC–LH1 complex to assemble in the dimeric form [10].

Second, with respect to the proposal that the two helices of PufX are at symmetrical positions away from the dimer interface (~100 Å apart), such an arrangement would preclude an interaction between the two PufX proteins if the helix adopts a straight conformation, and it is difficult to envisage how PufX could influence the formation or stability of the RC–LH1 dimer. However, the helix–bend–helix conformation would allow the N-terminal regions of PufX to interact with each other, or with the LH1 polypeptides, at the dimer interface [4]. These considerations raise the obvious question of whether the helix of PufX is straight or bent, and whether there is evidence that the N-terminus of PufX plays an important structural or functional role [4,6,39].

4.1. The structure of the PufX polypeptide

Before considering the new data described in the present report, it is of note that there is a striking contrast between the two published NMR structures of PufX, even though both were acquired in the same $CD_3OH/CDCl_3$ solvent system. The difference is limited to a small number of residues around Gly29, accepted to be in a helical region. On the one hand, it was concluded that residues 28–35 form part of a regular α-helix [3], while other work reached a different conclusion, that residues 29–34 form a bend between two continuous helices [2]. Interpretation of the amide proton exchange data differed for this region, which is more rapid than elsewhere in the helix. Tunnicliffe et al. [2] suggested that this observation required a bend in the helix, while Wang et al. [3] explained the amide-proton exchange as a consequence of the smaller side-chains in this region allowing faster access of solvent. However, this explanation is unlikely in view of the observation that the rate of amide proton exchange is not related to their degree of exposure to solvent but to the persistence of their hydrogen bonding [42,43]. The bend is expected to weaken hydrogen bonds in this region of the structure, which will increase the rate of hydrogen bond opening and result in increased amide-proton exchange.

A possibly crucial difference between the two studies is that Wang et al. [3] were restricted to data obtained with a 400 MHz

spectrometer, whereas Tunnicliffe et al. [2] used data obtained with 600 and 800 MHz spectrometers. The higher field strength and greater resolution in the latter work allowed the assignment of almost twice as many Nuclear Overhauser Effect (NOE)s, including more than twice as many longer range NOEs, which are the most important category in structure determination. A number of statistical measures of structure quality published in the two papers suggest that the linear PufX structure may have been rather over-restrained, probably as a result of the paucity of experimental data: for example, poorer (φ, ψ) distribution, higher energy, more restrictive hydrogen bond restraints, and greater NOE violations.

Fig. 1A shows that the T_2 relaxation rates obtained with PufX in organic solvent, which gave rise to the bent structure [2], are compatible with the HNCA intensities for PufX in a Zwittergent 3-14 micelle. Thus, the bent PufX structure is consistent with NMR data recorded in both solvent and micellar environments, and Fig. 1 shows how, in such a structure, it is possible for residues 17–54 (pale blue box) to be conformationally restricted, with only the N- and C-termini of the polypeptide showing significant mobility. The dark blue box shows the 21-residue α-helical region assigned in [3]. In the micelle-bound PufX structure in Fig. 1B the long N-terminal helix is anchored to the micelle through Trp21, which is conserved in all but one of the five PufX sequences (see Fig. 2A). Basic residues such as Lys15 and Arg19 are oriented with their side-chains capable of projecting out into the solvent. These new structural data prompted a re-evaluation of three aspects of the bent PufX structure: the N-terminal helix, the absolutely conserved residue Gly29 on the inside of the bend, and the C-terminus. These will be discussed in turn.

4.2. The consequence of a bent PufX structure: the role of the cytoplasmic N-terminal domain in promoting dimerisation of the core complex

In 2002, Francia and co–workers established the importance of the N-terminal region for the stability and function of PufX [6]. The present work confirms and extends their observations, showing that loss of the N-terminal sequence ADKTIFN through the ΔN-7 mutation results in a significant loss of dimers, and that more extensive loss of the residues ADKTIFNDHLNT through the ΔN-12 mutation abolishes dimer formation. This conclusion was verified by AFM analysis of membranes from the ΔN-12 mutant, where only monomeric core complexes were imaged.

A consequence of the bend in the helix of PufX is that it would allow the N-terminal residues ADKTIFNDHLNT from opposing PufX molecules, which are required for core dimerisation, to extend towards the dimer interface, while allowing the membrane-spanning helices of each PufX to be located several tens of ångströms away from the interface, as assigned in the projection density map in [4]. The contact could either be directly between PufX proteins or, more likely, with surface LH1 residues on the other half of the dimer. Such an interaction is modelled in Fig. 7, which shows a structural model of the RC–LH1–PufX dimer complex, based on the 8.5 Å projection map [4], and modeling studies [44–46], incorporating a conformation of the solution structure of PufX [2] with an extended N-terminus. We note that this model of the dimer complex in Fig. 7 does not take into account interactions with lipid and with other proteins, which most likely play a role in determining the functional structure of the N-terminal region of PufX in the native membrane. Nevertheless, the

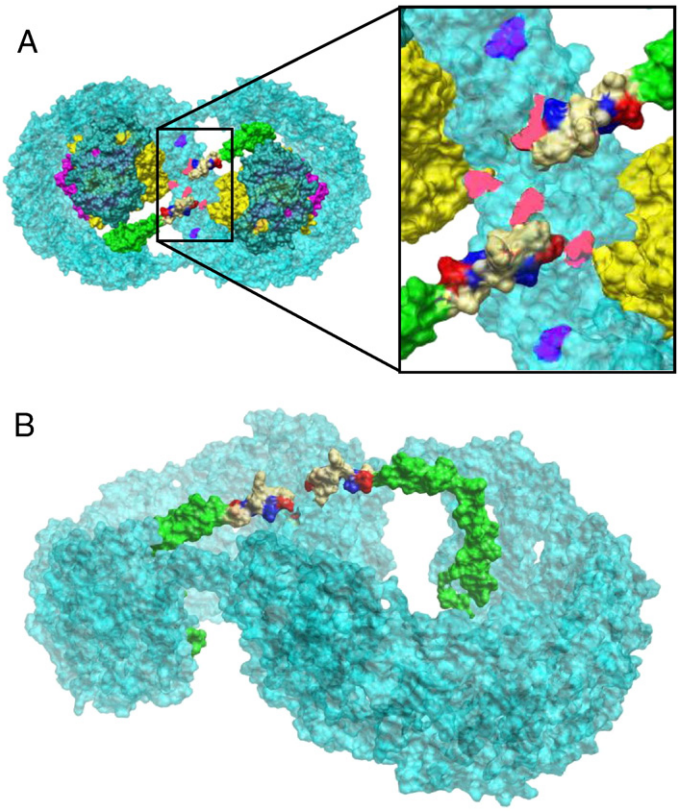

Fig. 7. A model of interaction between PufX polypeptide and LH1 subunits in the dimeric core complex from *Rba. sphaeroides*. The model is based on a calculation from a molecular dynamics flexible fitting (MDFF) simulation of the RC–LH1 dimer [45,46] using a conformer of PufX from the determination of the solution structure with an extended N-terminus [2]. (A) Projection view of the dimer model from the cytoplasmic side: LH1 is in cyan, and the RC H, L and M subunits are in blue–green, yellow and magenta, respectively; PufX is in green with the 12 N-terminal residues in khaki. Red and blue are used to label the positively- and negatively-charged sidechains in the 12-residue N-terminal region of the PufX, while pink and purple are used for positively- and negatively-charged side-chains of the cytoplasmic surface of the LH1 α and β polypeptides, but only in the central region at the dimer interface. (B) A different viewing angle of the model with the RCs removed for clarity to show the bend in PufX and using the PufX location proposed by [4]. The images were produced using the UCSF Chimera package from the Resource for Biocomputing, Visualization, and Informatics at the University of California, San Francisco [66].

projection view of the structural model in Fig. 7A shows how the extended N-terminus of PufX from one half of the dimer is sufficiently long to reach over to the LH1 complex on the other half. Fig. 7B shows a 3-D representation of the model with the RCs omitted, to emphasise the capacity of the N-terminus of PufX to bridge across to the other half of the dimer. In both Fig. 7A and B, the first 12 residues of PufX are colored in khaki, to show how it is possible for deletion of the N-terminal sequence ADKTIFNDHLNT through the ΔN-12 mutation to abolish dimer formation.

It is already known that the sequence ADKTIFN at the N-terminus of PufX is sufficiently exposed on the cytoplasmic side of the core dimer complex to be susceptible to proteolytic digestion [11]; furthermore, the N-terminal deletions show that the sequence ADKTIFNDHLNT is required for dimerisation. Taken together, these observations suggest that charged residues on PufX and on the LH1α and β polypeptides on the cytoplasmic face of the dimer complex might mediate the surface association of the N-terminus of PufX with the cytoplasmic surface of LH1. It is possible that the Asp and Lys residues in the ADKTIFNDHLNT PufX sequence interact with ionised residues on the N-terminus of LH1α (MSKFYKIWMIFDPRR) and/or β (ADKSDLGYTGLTDE), as depicted in the inset in Fig. 7A.

4.3. The consequence of a bent PufX structure: requirement for the strictly conserved residue Gly29 to allow the bend to form, allowing stable assembly of PufX into the core complex

As outlined above, Gly29 is one of only eight residues absolutely conserved in the five available sequences for PufX proteins, six of them at the C-terminal end of the transmembrane helix. The bent structure for PufX suggests a reason for the conservation of this Gly, as this is the only residue small enough to fit into the inside of the bend at this position while avoiding steric clashes with neighbouring amino acids. The experimental data outlined above indicate that increasing the volume of the side-chain at this position through the series Ala → Val → Leu/Ile had increasingly strong effects on the properties of the RC–LH1 complex, manifested as decreases in the population of dimers, loss of PufX from the membrane, increases in the amount of LH1 bacteriochlorophyll per RC and impaired capacity for photosynthetic growth. The data would indeed suggest that the size of the side-chain at position 29 is a critical factor for assembly of PufX into the membrane and into the RC–LH1 complex.

To provide additional insights, Fig. 8 shows a series of structural models which explore the consequences of enlarging Gly29, using the bent conformation of PufX [2] shown in Fig. 1. The overall fold of PufX is shown using a green ribbon, and the α-carbon of Gly29 is shown as a magenta sphere. Also shown as spheres are the amino acids Gln25 and Ala33, which are on the same side of the helix as Gly29 (carbons coloured yellow, oxygens red and nitrogens blue). Fig. 8A shows a view from inside the bend of the effect of changing Gly29 to Ala or Val, showing the preferred conformer in each case, while Fig. 8B shows a side-on view of the consequences of changing Gly29 (left) to Ile (middle). The models indicate that increasing the volume of the side chain at position 29 brought about increasing amounts of steric overlap with atoms of the neighbouring amino acids, particularly Gln25, the affected atoms being coloured orange in Fig. 8B. Avoidance of this clash necessitated a widening of the bend, with PufX pivoting at the α-carbon at position 29 in a direction away from the plane of the membrane (shown for the Ile model in Fig. 8B, panel on right). Therefore, it would appear that Gly is the only residue at this position that permits the correct degree of bending which, we suggest, is required to allow Trp21 close enough to the membrane surface to act as a membrane anchor, and to allow the N-terminus to reach across to the dimer interface. Thus, the bend is essential for the stable assembly of PufX into the core complex.

In contrast, when the same modeling exercise was performed using the linear model for PufX [3] and Gly29 was replaced with Ile or Leu, the larger side-chains were tolerated (not shown) since there was at least one possible rotamer for either Leu or Ile where there was minimal steric overlap with neighbouring atoms. For other rotamers, much of the overlap could be overcome by movement of adjacent side-chains. In conclusion, the mutagenesis data demonstrate that side-chains larger than glycine are not tolerated at position 29, and that the bent conformation of PufX, but not the linear conformation, provides a structural explanation for the effects of the mutations.

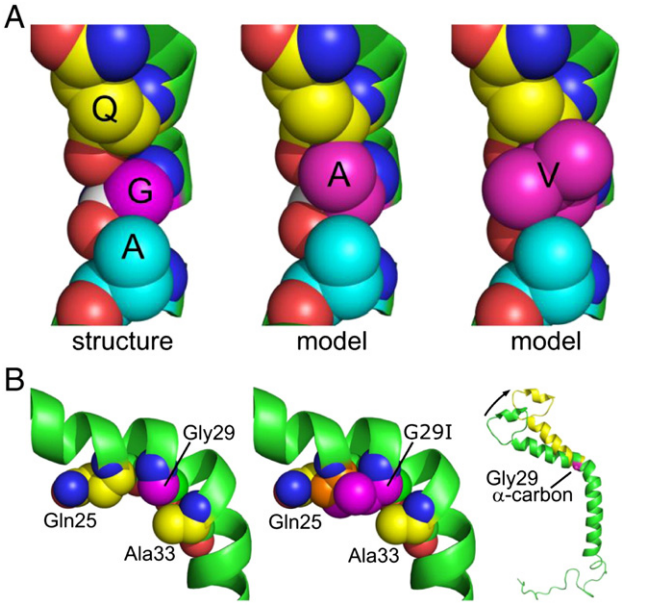

Fig. 8. Modelling of the consequences of enlargement of the X29 residue on the overall fold of PufX. (A) Models of PufX (green ribbon) in the region of Gly29, viewed from inside the bend. On the left, amino acids Gln25 (yellow carbons), Ala33 (cyan carbons) and Gly29 (magenta carbons) are shown as spheres; oxygens and nitrogens are shown in red and blue, respectively; in the middle and right are *in silico* models of G29A and G29V mutations, showing steric overlap with the adjacent Gln and Ala residues. (B) Left: view of Gly29, normal to the 120° bend in the membrane-spanning helix of PufX (green ribbon). Gly29 is shown as spheres with a magenta α-carbon, Gln25 and Ala33 are shown as spheres with yellow side-chain and α-carbons. Middle: equivalent view of a model with Gly29 replaced by Ile. Atoms of Gln25 that engage in steric clashes with the Ile29 side chain are highlighted as orange spheres. This side-on view illustrates how increasing the volume of this conserved Gly residue at position 29 will cause steric clashes with Gln25, and would prevent PufX from adopting this 120° bent helix conformation. Right: ribbon model of PufX (green), showing the position of Gly29 (magenta) on the inside of the bend in the PufX helix. The α-carbon of Gly29 is shown as a sphere. The yellow ribbon indicates the degree to which the 1–29 region of PufX would have to be pivoted around the α-carbon of residue 29, in a direction normal to the plane of the membrane, to alleviate the side-chain to side-chain clashes between Gln25 and Ile29 illustrated in the middle panel.

4.4. The C-terminus of PufX

There are no major differences between the bent and linear structural models of PufX in terms of the C-terminal residues. In both cases the periplasmic end of the central helix finishes at residue Met53 and the C-terminus is largely unstructured. However, it was reported, on the basis of mass spectrometry data and determination of the C-terminal amino acid, that processing removes 12 amino acids from the C-terminus of the *Rba. sphaeroides* PufX [13]. This observation is not consistent with experiments making use of a C-terminal (His_6) tag to quantify the RC:PufX stoichiometry, where processing was not seen [14]. In the latter case the LH1 and LH2 antenna complexes were present, while in the work of Parkes-Loach et al. [13] an $LH1^-/LH2^-$ strain was used, leading to suggestion that the presence of LH2 could influence the processing of PufX [6].

Reasons for this discrepancy could certainly have included the presence of LH2, but also could include an influence of the His_6 tag, non-specific proteolysis of PufX upon cell disruption, and variations in the stage of pigmentation of cultures. To circumvent these difficulties, in readdressing this issue of processing of the C-terminus we used cells with or without LH2, and two different tags, either T7 or His_6. Furthermore experiments were conducted on whole cells with no membrane preparation involved, and on cells undergoing a shift from an unpigmented to a fully pigmented state. In summary, regardless of all these factors, clear evidence was obtained for C-terminal processing. The remaining difference between our studies and those of [14] is that in the present work plasmid-borne *pufBALMX* genes were used to complement *puf* deletion mutants to introduce a tagged PufX, whereas Francia et al. [14] used a more rigorous approach in which the complementing *pufX* gene was integrated into the chromosome. Nevertheless, we conclude that the PufX C-terminus is processed, although the underlying reason for this is not clear. The insertion of nascent PufX into the membrane might require the C-terminal sequence LETGIELIKHLV, but its subsequent removal might be essential for efficient functioning of the core dimer, perhaps to allow docking of the cytochrome c_2 on the periplasmic face of the RC [47]. Certainly the PufX C-terminal region appears to be important for membrane insertion of PufX and its assembly into the core complex [6].

5. Conclusions

The function of PufX appears to involve a role in promoting quinol/quinone exchange, prior to reduction of the cytochrome bc_1 complex. First, it is necessary for quinols generated at the RC Q_B site to equilibrate with an internal quinol/quinone pool; the absence of PufX perturbs the kinetics of quinone/quinol exchange at the RC Q_B site, with concomitant effects on the Q_A site and charge separation [48–51]. An internal quinone pool (actually two, one for each RC), of 10–15 quinone molecules has been proposed within the dimer complex on the basis of biochemical analyses [52]. Subsequent 3-D reconstruction of the dimer complex identified a space in the structure adjacent to each RC, large enough to accommodate approximately 10 quinone molecules [5]. Each of the two spaces in the dimer space can been as an empty cavity in the model in Fig. 7A, adjacent to the most easily breached part of the LH1 ring. The two internal quinone pools identified in [52] must equilibrate with the external pool as part of the eventual diffusion of quinol towards the cytochrome bc_1 complex, a process which requires exchange of quinols and quinones across the encircling LH1 ring. It has been proposed, on the basis of relatively weak and diffuse electron density at the 14th LH1 αβ pair, that this part of the LH1 ring, which is close to PufX, is most easily breached [4]. Although more structural information is required, the fact that on each half of the core dimer the RC Q_B site, the proposed internal quinone pool, PufX, and the 14th LH1 αβ pair are all found within a relatively restricted area is suggestive of a functional linkage between these components.

None of the above would appear to require dimeric, as opposed to monomeric, RC–LH1–PufX core complexes, and indeed bacteria such as *Rhodopseudomonas palustris* and *Rba. veldkampii* have a monomeric core complex with a PufX analog [39,53–55]. Monomeric cores and LH2 complexes appear to associate in the membrane fairly randomly (for example, [56,57]), whereas core dimers, with their membrane-bending properties and elongated shape [4,5], induce partitioning of dimers and LH2 complexes into distinct domains [37,58]. This process has been simulated using a colloid model, with size and curvature mismatches between dimers and LH2 complexes as the drivers of dimer-rich and LH2-rich domains [59]. Earlier linear dichroism studies had already shown how the loss of PufX can remodel the whole shape and organisation of the photosynthetic membrane [60,61]; the AFM data in this paper show how the loss of only 12 residues from the PufX N-terminus has similar effects on membrane organisation. The link between the organisation of a membrane and its ability to function in converting light into ATP is still far from clear, although a combination of AFM and functional studies, allied to *in silico* modelling of whole membranes, provides insights into this relationship [62,63]. Thus, there is a role for PufX beyond quinone/quinol equilibration, with PufX-mediated dimerisation of core complexes leading to partitioning of the membrane into distinct core- and LH2-rich domains, and this organised arrangement contributing in some way to trafficking of quinols to the cytochrome bc_1 complex [64].

Acknowledgments

ECR, PQ, CNH, RBT and MPW acknowledge financial support from the Biotechnology and Biological Sciences Research Council (UK). CNH was supported as part of the Photosynthetic Antenna Research Center (PARC), an Energy Frontier Research Center funded by the U.S. Department of Energy, Office of Science, Office of Basic Energy Sciences under Award Number DE-SC 0001035. MRJ acknowledges financial support from The Royal Society (UK). IWN, KHD and PGA acknowledge doctoral studentships from the Biotechnology and Biological Sciences Research Council (UK). We thank HEFCE/JREI for NMR instrument support.

References

[1] K. Holden-Dye, L.I. Crouch, M.R. Jones, Structure, function and interactions of the PufX protein, Biochim. Biophys. Acta 1777 (2008) 613–630.
[2] R.B. Tunnicliffe, E.C. Ratcliffe, C.N. Hunter, M.P. Williamson, The solution structure of the PufX polypeptide from *Rhodobacter sphaeroides*, FEBS Lett. 580 (2006) 6967–6971.
[3] Z.Y. Wang, H. Suzuki, M. Kobayashi, T. Nozawa, Solution structure of the *Rhodobacter sphaeroides* PufX membrane protein: implications for the quinone exchange and protein–protein interactions, Biochemistry 46 (2007) 3635–3642.
[4] P. Qian, C.N. Hunter, P.A. Bullough, The 8.5 Å projection structure of the core RC–LH1–PufX dimer of *Rhodobacter sphaeroides*, J. Mol. Biol. 349 (2005) 948–960.
[5] P. Qian, P.A. Bullough, C.N. Hunter, Three-dimensional reconstruction of a membrane-bending complex, J. Biol. Chem. 283 (2008) 14002–14011.
[6] F. Francia, J. Wang, H. Zischka, G. Venturoli, D. Oesterhelt, Role of the N- and C-terminal regions of the PufX protein in the structural organization of the photosynthetic core complex of *Rhodobacter sphaeroides*, Eur. J. Biochem. 269 (2002) 1877–1885.
[7] J.M. Busselez, M. Cottevieille, P. Cuniasse, F. Gubellini, N. Boisset, D. Lévy, Structural basis for the PufX-mediated dimerization of bacterial photosynthetic core complexes, Structure 15 (2007) 1674–1683.
[8] W.P. Russ, D.M. Engelman, The GxxxG motif: a framework for transmembrane helix–helix association, J. Mol. Biol. 296 (2000) 911–919.
[9] J. Hsin, C. Chipot, K. Schulten, A glycophorin a-like framework for the dimerization of photosynthetic core complexes, J. Am. Chem. Soc. 131 (2009) 17096–17098.
[10] L.I. Crouch, K. Holden-Dye, M.R. Jones, Dimerisation of the *Rhodobacter sphaeroides* RC–LH1 photosynthetic complex is not facilitated by a GxxxG motif in the PufX polypeptide, Biochim. Biophys. Acta 1797 (2010) 1812–1819.
[11] R.J. Pugh, P. McGlynn, M.R. Jones, C.N. Hunter, The LH1-RC core complex of *Rhodobacter sphaeroides*: interaction between components, time-dependent assembly, and topology of the PufX protein, Biochim. Biophys. Acta 1366 (1998) 301–316.
[12] J.K. Lee, B.S. DeHoff, T.J. Donohue, R.I. Gumport, S. Kaplan, Transcriptional analysis of *puf* operon expression in *Rhodobacter sphaeroides* 2.4.1. and an intercistronic transcription terminator mutant, J. Biol. Chem. 264 (1989) 19354–19365.
[13] P.S. Parkes-Loach, C.J. Law, P.A. Recchia, J. Kehoe, S. Nehrlich, J. Chen, P.A. Loach, Role of the core region of the PufX protein in inhibition of reconstitution of the core light-harvesting complexes of *Rhodobacter sphaeroides* and *Rhodobacter capsulatus*, Biochemistry 40 (2001) 5593–5601.
[14] F. Francia, J. Wang, G. Venturoli, B.A. Melandri, W.P. Barz, D. Oesterhelt, The reaction center-LH1 antenna complex of *Rhodobacter sphaeroides* contains one PufX molecule which is involved in dimerization of this complex, Biochemistry 38 (1999) 6834–6845.
[15] P.L. Sorgen, S.M. Cahill, R.D. Krueger-Koplin, S.T. Krueger-Koplin, C.C. Schenck, M.E. Girvin, Structure of the *Rhodobacter sphaeroides* light-harvesting 1 beta subunit in detergent micelles, Biochemistry 41 (2002) 31–41.
[16] F.W. Studier, Protein production by auto-induction in high-density shaking cultures, Protein Expr. Purif. 41 (2005) 207–234.
[17] P.A. Recchia, C.M. Davis, T.G. Lilburn, J.T. Beatty, P.S. Parkes-Loach, C.N. Hunter, P.A. Loach, Isolation of the PufX protein from *Rhodobacter capsulatus* and *Rhodobacter sphaeroides*: evidence for its interaction with the α-polypeptide of the core light-harvesting complex, Biochemistry 37 (1998) 11055–11063.

[18] K.A. Meadows, K. Iida, K. Tsuda, P.A. Recchia, B.A. Heller, B. Antonio, M. Nango, P.A. Loach, Enzymatic and chemical cleavage of the core light-harvesting polypeptides of photosynthetic bacteria: determination of the minimal polypeptide size and structure required for subunit and light-harvesting complex formation, Biochemistry 34 (1995) 1559–1574.
[19] M.A.C. Reed, A.M. Hounslow, K.H. Sze, I.G. Barsukov, L.L.P. Hosszu, A.R. Clarke, C.J. Craven, J.P. Waltho, Effects of domain dissection on the folding and stability of the 43 kDa protein PGK probed by NMR, J. Mol. Biol. 330 (2003) 1189–1201.
[20] R.A. Niederman, D.E. Mallon, J.J. Langan, Membranes of *Rhodopseudomonas sphaeroides*. IV. Assembly of chromatophores in low-aeration cell suspensions, Biochim. Biophys. Acta 440 (1976) 429–447.
[21] K. Holden-Dye, Biophysical studies of photosynthetic membrane proteins from Rhodobacter sphaeroides, PhD Thesis (2007) University of Bristol.
[22] C.N. Hunter, P. McGlynn, M.K. Ashby, J.G. Burgess, J.D. Olsen, DNA sequencing and complementation/deletion analysis of the *bchA-puf* operon region of *Rhodobacter sphaeroides*: *in vivo* mapping of the oxygen-regulated *puf* promoter, Mol. Microbiol. 5 (1991) 2649–2661.
[23] M.R. Jones, G.J.S. Fowler, L.C.D. Gibson, G.G. Grief, J.D. Olsen, W. Crielaard, C.N. Hunter, Mutants of *Rhodobacter sphaeroides* lacking one or more pigment–protein complexes and complementation with reaction-centre, LH1, and LH2 genes, Mol. Microbiol. 6 (1992) 1173–1184.
[24] C.N. Hunter, G. Turner, Transfer of genes coding for apoproteins of reaction center and light-harvesting LH1 complexes to *Rhodobacter sphaeroides*, J. Gen. Microbiol. 134 (1988) 1471–1480.
[25] H. Schägger, G. von Jagow, Tricine-sodium dodecyl sulfate-polyacrylamide gel electrophoresis for the separation of proteins in the range from 1 to 100 kDa, Anal. Biochem. 166 (1987) 368–379.
[26] J. Sambrook, E.F. Fritsch, T. Maniatis, Molecular Cloning, 2nd edn., A Laboratory Manual, Cold Spring Harbor Laboratory Press, Cold Spring Harbor, NY, 1989.
[27] J. Cavanagh, W.J. Fairbrother, A.G. Palmer, M. Rance, N.J. Skelton, Protein NMR spectroscopy, Academic Press, Oxford, 2007.
[28] J. Lipfert, L. Columbus, V.B. Chu, S.A. Lesley, S. Doniach, Size and shape of detergent micelles determined by small-angle X-ray scattering, J. Phys. Chem. B 111 (2007) 12427–12438.
[29] Y. Tsukatani, K. Matsuura, S. Masuda, K. Shimada, A. Hiraishi, K.V.P. Nagashima, Phylogenetic distribution of unusual triheme to tetraheme cytochrome subunit in the reaction center complex of purple photosynthetic bacteria, Photosyn. Res. 79 (2004) 83–91.
[30] G. Klug, S.N. Cohen, Pleiotropic effects of localized *Rhodobacter capsulatus puf* operon deletions on production of light-absorbing pigment-protein complexes, J. Bacteriol. 170 (1988) 5814–5821.
[31] J.W. Farchaus, H. Gruenberg, D. Oesterhelt, Complementation of a reaction center-deficient *Rhodobacter sphaeroides pufLMX* deletion strain in *trans* with *pufBALM* does not restore the photosynthesis-positive phenotype, J. Bacteriol. 172 (1990) 977–985.
[32] T.G. Lilburn, C.E. Haith, R.C. Prince, J.T. Beatty, Pleiotropic effects of *pufX* gene deletion on the structure and function of the photosynthetic apparatus of *Rhodobacter capsulatus*, Biochim. Biophys. Acta 1100 (1992) 160–170.
[33] P. McGlynn, C.N. Hunter, M.R. Jones, The *Rhodobacter sphaeroides* PufX protein is not required for photosynthetic competence in the absence of a light harvesting system, FEBS Lett. 349 (1994) 349–353.
[34] P. McGlynn, W.H.J. Westerhuis, M.R. Jones, C.N. Hunter, Consequences for the organisation of reaction center-light harvesting antenna 1 (LH1) core complexes of *Rhodobacter sphaeroides* arising from deletion of amino acid residues from the C terminus of the LH1 α polypeptide, J. Biol. Chem. 271 (1996) 3285–3292.
[35] T.K. Fulcher, J.T. Beatty, M.R. Jones, A demonstration of the key role played by the PufX protein in the functional and structural organisation of native and hybrid bacterial photosynthetic core complexes, J. Bacteriol. 180 (1998) 642–646.
[36] S. Scheuring, J. Seguin, S. Marco, D. Lévy, B. Robert, J.L. Rigaud, Nanodissection and high-resolution imaging of the *Rhodopseudomonas viridis* photosynthetic core complex in native membranes by AFM, Proc. Natl. Acad. Sci. U. S. A. 100 (2003) 1690–1693.
[37] S. Bahatyrova, R.N. Frese, C.A. Siebert, J.D. Olsen, K.O. van der Werf, R. van Grondelle, R.A. Niederman, P.A. Bullough, C. Otto, C.N. Hunter, The native architecture of a photosynthetic membrane, Nature 430 (2004) 1058–1062.
[38] J.N. Sturgis, J.D. Tucker, J.D. Olsen, C.N. Hunter, R.A. Niederman, Atomic force microscopy studies of native photosynthetic membranes, Biochemistry 48 (2009) 3679–3698.
[39] P.A. Bullough, P. Qian, C.N. Hunter, Reaction center-light harvesting core complexes of purple bacteria, in: C.N. Hunter, F. Daldal, M.C. Thurnauer, J.T. Beatty (Eds.), The Purple Phototrophic Bacteria, Springer, Dordrecht, The Netherlands, 2009, pp. 155–179.
[40] S. Scheuring, F. Francia, J. Busselez, B.A. Melandri, J.L. Rigaud, D. Lévy, Structural role of PufX in the dimerization of the photosynthetic core-complex of *Rhodobacter sphaeroides*, J. Biol. Chem. 279 (2004) 3620–3626.
[41] S. Scheuring, J. Busselez, D. Lévy, Structure of the dimeric PufX-containing core complex of *Rhodobacter blasticus* by *in situ* atomic force microscopy, J. Biol. Chem. 280 (2005) 1426–1431.
[42] M.A. Contreras, T. Haack, M. Royo, E. Giralt, M. Pons, Temperature coefficients of peptides dissolved in hexafluoroisopropanol monitor distortions of helices, Lett. Pept. Sci. 4 (1997) 29–39.
[43] S.W. Englander, Protein folding intermediates studied by hydrogen exchange, Ann. Rev. Biophys. Biomol. Struct. 29 (2000) 213–238.
[44] D. Fotiadis, P. Qian, A. Philippsen, P.A. Bullough, A. Engel, C.N. Hunter, Structural analysis of the RC–LH1 photosynthetic core complex of *Rhodospirillum rubrum* using atomic force microscopy, J. Biol. Chem. 279 (2004) 2063–2068.
[45] D.E. Chandler, J. Hsin, C.B. Harrison, J. Gumbart, K. Schulten, Intrinsic curvature properties of photosynthetic proteins in chromatophores, Biophys. J. 95 (2008) 2822–2836.
[46] J. Hsin, J. Gumbart, L.G. Trabuco, E. Villa, P. Qian, C.N. Hunter, K. Schulten, Protein-induced membrane curvature investigated through molecular dynamics flexible fitting, Biophys. J. 97 (2009) 321–329.
[47] H.L. Axelrod, E.C. Abresch, M.Y. Okamura, A.P. Yeh, D.C. Rees, G. Feher, X-ray structure determination of the cytochrome c_2: reaction center electron transfer complex from *Rhodobacter sphaeroides*, J. Mol. Biol. 319 (2002) 501–515.
[48] W.P. Barz, F. Francia, G. Venturoli, B.A. Melandri, A. Verméglio, D. Oesterhelt, Role of the PufX protein in photosynthetic growth of *Rhodobacter sphaeroides*. 1. PufX is required for efficient light-driven electron transfer and photophosphorylation under anaerobic conditions, Biochemistry 34 (1995) 15235–15247.
[49] W.P. Barz, A. Verméglio, F. Francia, G. Venturoli, B.A. Melandri, D. Oesterhelt, Role of the PufX protein in photosynthetic growth of the *Rhodobacter sphaeroides*. 2. PufX is required for efficient ubiquinone/ubiquinol exchange between the reaction center Q_B site and the cytochrome bc_1 complex, Biochemistry 34 (1995) 15248–15258.
[50] R. Comayras, C. Jungas, J. Lavergne, Functional consequences of the organization of the photosynthetic apparatus in *Rhodobacter sphaeroides*—II. A study of $PufX^-$ membranes, J. Biol. Chem. 280 (2005) 11214–11223.
[51] R. Comayras, C. Jungas, J. Lavergne, Functional consequences of the organization of the photosynthetic apparatus in *Rhodobacter sphaeroides*—I. Quinone domains and excitation transfer in chromatophores and reaction center antenna complexes, J. Biol. Chem. 280 (2005) 11203–11213.
[52] M. Dezi, F. Francia, A. Mallardi, G. Colafemmina, G. Palazzo, G. Venturoli, Stabilization of charge separation and cardiolipin confinement in antenna–reaction center complexes purified from *Rhodobacter sphaeroides*, Biochim. Biophys. Acta 1767 (2007) 1041–1056.
[53] A.W. Roszak, T.D. Howard, J. Southall, A.T. Gardiner, C.J. Law, N.W. Isaacs, R.J. Cogdell, Crystal structure of the RC–LH1 core complex from *Rhodopseudomonas palustris*, Science 302 (2003) 1969–1972.
[54] F. Gubellini, F. Francia, J. Busselez, G. Venturoli, D. Lévy, Functional and structural analysis of the photosynthetic apparatus of *Rhodobacter veldkampii*, Biochemistry 45 (2006) 10512–10520.
[55] L.-N. Liu, J.N. Sturgis, S. Scheuring, Native architecture of the photosynthetic membrane from *Rhodobacter veldkampii*, J. Struct. Biol. doi:10.1016/j.jsb.2010.08.010.
[56] S. Scheuring, J.L. Rigaud, J. Sturgis, Variable LH2 stoichiometry and core clustering in native membranes of *Rhodospirillum photometricum*, EMBO J. 23 (2004) 4127–4133.
[57] S. Scheuring, J.N. Sturgis, Chromatic adaption of photosynthetic membranes, Science 309 (2005) 484–487.
[58] J.D. Tucker, C.A. Siebert, M. Escalante, P.G. Adams, J.D. Olsen, C. Otto, D.L. Stokes, C.N. Hunter, Membrane invagination in *Rhodobacter sphaeroides* is initiated at curved regions of the cytoplasmic membrane, then forms both budded and fully detached spherical vesicles, Mol. Microbiol. 76 (2010) 833–847.
[59] R.N. Frese, J.C. Pamies, J.D. Olsen, S. Bahatyrova, C.D. van der Weij-de Wit, T.J. Aartsma, C. Otto, C.N. Hunter, D. Frenkel, R. van Grondelle, Protein shape and crowding drive domain formation and curvature in biological membranes, Biophys. J. 94 (2008) 640–647.
[60] R.N. Frese, J.D. Olsen, R. Branvall, W.H. Westerhuis, C.N. Hunter, R. van Grondelle, The long-range supraorganization of the bacterial photosynthetic unit: a key role for PufX, Proc. Natl. Acad. Sci. U. S. A. 97 (2000) 5197–5202.
[61] R.N. Frese, C.A. Siebert, R.A. Niederman, C.N. Hunter, C. Otto, R. van Grondelle, The long-range organization of a native photosynthetic membrane, Proc. Natl. Acad. Sci. U. S. A. 101 (2004) 17994–17999.
[62] M.K. Şener, K. Schulten, From atomic-level structure to supramolecular organization in the photosynthetic unit of purple bacteria, in: C.N. Hunter, F. Daldal, M.C. Thurnauer, J.T. Beatty (Eds.), The Purple Phototrophic Bacteria, Springer, Dordrecht, The Netherlands, 2009, pp. 275–294.
[63] M.K. Şener, J.D. Olsen, C.N. Hunter, K. Schulten, Atomic level structural and functional model of a bacterial photosynthetic membrane vesicle, Proc. Natl. Acad. Sci. U. S. A. 104 (2007) 15273–15278.
[64] J. Lavergne, A. Verméglio, P. Joliot, Functional coupling between reaction centers and cytochrome bc_1 complexes, in: C.N. Hunter, F. Daldal, M.C. Thurnauer, J.T. Beatty (Eds.), The Purple Phototrophic Bacteria, Springer, Dordrecht, The Netherlands, 2009, pp. 509–536.
[65] M. Schiffer, C.H. Chang, F.J. Stevens, The functions of tryptophan residues in membrane proteins, Protein Eng. 5 (1992) 213–214.
[66] E.F. Pettersen, T.D. Goddard, C.C. Huang, G.S. Couch, D.M. Greenblatt, E.C. Meng, T.E. Ferrin, UCSF Chimera—a visualization system for exploratory research and analysis, J. Comput. Chem. 25 (2004) 1605–1612.